Dynamic and Static Fluorescence Spectroscopy Applied to Miscibility of Poly(*n*-butyl methacrylate-*co*-styrene) with Polystyrene and Morphological Analysis by Epifluorescence Microscopy

Marcelo L. de Andrade and Teresa D. Z. Atvars*

Instituto de Química, Universidade Estadual de Campinas, Campinas, São Paulo Caixa Postal 6154, Campinas, CEP 13084-971, SP, Brazil

Received: March 14, 2003; In Final Form: January 21, 2004

The microphase structure in blends of poly(*n*-butyl methacrylate-*co*-styrene) (nBMAS) and polystyrene (PS) was investigated by nonradiative energy transfer (NRET) using both steady-state fluorescence and time correlated single-photon counting (TCSPC) measurements. The nBMAS was labeled with anthryl groups by semicontinuous emulsion copolymerization. Studies of the morphology and phase separation of these blends performed by epifluorescence microscopy were complemented by differential scanning calorimetry. Miscibility of polymers with several compositions, from 5 to 95% w/w, was studied. For compositions with PS < 80 wt % we obtained a partial miscibility with discrete domains of PS dispersed in a nBMAS matrix. Blends up to PS = 20 wt % presented a co-continuous morphology whereas a bicontinuous morphology was generated for lower PS content. Fluorescence lifetimes and the lifetime distribution were consistently associated with the microheterogeneity of the material and were considered an additional criterion for the analysis of miscibility.

Introduction

Blending polymers (miscible and immiscible) is an issue of great interest because it can be a less expensive way to create materials with the desired properties. From the fundamental point of view they are ideal systems for studies of the phase-separation phenomena and how it influences macroscopic properties. Nevertheless, among all the possible combinations of existing polymers, miscible blends are a rather a small group because of poor interaction between the components.

Lacking any special functional groups in its chain structure, polystyrene (PS) is immiscible with most long-chain thermoplastic polymers. Blends of PS with ester-containing polymers or acrylic polymers (having carbonyl groups) have been considered mostly immiscible, at least on the basis of thermal property criteria. Many reported results have proven that the miscibility in blends of PS with acrylic polymers can be substantially enhanced by introducing a certain amount of some molecular groups or ions that are capable of establishing strong interactions, such as hydrogen bonding[1−3] or ion−ion[4] interaction between the polymeric pairs. Several studies emphasized that the copolymerization of acrylic (or methacrylic) monomers with styrene can enhance the miscibility of polymer blends of PS and acrylic polymers.[5−10] Results have been reported for relatively inexpensive materials with great design flexibility.

Usually, miscibility is evaluated by differential scanning calorimetry (DSC) or dynamic mechanical analysis (DMA),[11,12] on the basis of the existence of a single value of glass transition temperature (T_g). However, several different methods can be employed to investigate miscibility with different spatial resolutions. Techniques based on scattering (SAXS and SANS, as well as light scattering) were applied in numerous studies of phase stability and kinetics of phase separation in polymer blends.[2,3,7,8] For a better understanding of the degree of mixing, a good characterization of the spatial distribution of the two components on very small spatial scale is necessary. Solid state NMR[13] and fluorescence techniques,[1,14−17] including excimer formation and nonradiative energy transfer and combined techniques,[18,19] have been regarded as powerful methods for this purpose. Some advantages of using excimer fluorescence spectroscopy for studies of polymer−polymer miscibility[20,21] were reported: (i) the higher sensitivity of the technique, allowing studies at concentrations as low as 0.5 wt % and (ii) the utility of excimer formation as a sensor for the immediate environment around these groups, leading to the ability of monitoring molecular interpenetration on a scale much smaller than that possible with thermal techniques.

Furthermore, nonradiative energy transfer processes between a donor and an acceptor group (NRET) provide a powerful technique for studies of polymer interfaces and phase morphology, because these processes involve energy transfer from excited donors to acceptors, within a distance range of a few nanometers.[22] The basic idea supporting the NRET technique is the analysis of energy transfer from one polymer, containing donor moieties, to another polymer, containing acceptor moieties. Decreases of both the donor fluorescence intensity and its fluorescence lifetime are strong evidences that energy transfer to the acceptors is occurring, when they are separated by short distances.[1,15,23−26]

In the present work, the phase separation of a binary blend of PS, which contains phenyl groups as possible donors, and poly(*n*-butyl methacrylate-*co*-styrene) (nBMAS) labeled with anthryl units, as possible acceptor groups (Scheme 1), was studied. Blends were prepared with several PS compositions, from 5% to 95 wt %. Epifluorescence imaging microscopy (EFIM), steady-state fluorescence, and time-resolved spectroscopy techniques were used to investigate the morphology of films prepared by casting dilute solutions containing both

* Corresponding author. Fax: 55-19-37883023. Tel: 55-19-37883078. E-mail: tatvars@iqm.unicamp.br.

10.1021/jp034664h CCC: $27.50
Published on Web 03/09/2004

SCHEME 1: Chemical Structure of Poly(*n*-butyl methacrylate-*co*-styrene) (nBMAS) Labeled with 9-Anthryl Groups[a]

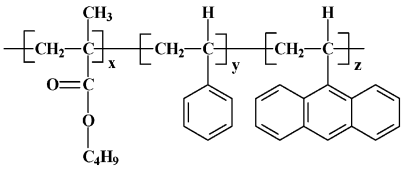

[a] *x*, *y*, and *z* are the approximate molar ratios determined by UV−vis absorption spectroscopy ($x = 0.775$; $y = 0.224$; $z = 0.001$).

polymers. The NRET processes can also be evaluated by steady-state fluorescence spectroscopy. Fluorescence lifetimes were determined and lifetime distribution was employed to analyze the experimental decay of the fluorescence emission. Intermolecular correlations among the donors and traps were used to analyze the interchain structures in homogeneous blends and in blends with phase separation.

Experimental Section

Chemicals. Monomers (*n*-butyl methacrylate, nBMA, Aldrich Chemical Co., and styrene, STY, Aldrich Chemical Co.) were washed with 5% sodium hydroxide, followed by distilled water. Afterward, they were first dried over anhydrous sodium sulfate, then purified by vacuum distillation, and stored in a refrigerator. The fluorescent monomer 9-vinylanthracene (9-VAn, 97%, Aldrich Chemical Co.), potassium persulfate (KPS, 99%, Aldrich Chemical Co.), sodium dodecyl sulfate (SDS, 98%, Merck), sodium bicarbonate (99%, Synth), and dodecyl mercaptan (DM, 99.5%, Aldrich) were used as supplied. Chloroform (Merck) and methanol (Merck) were of analytical grade. Atactic polystyrene (PS, $\bar{M}_w = 160$k) was purchase from EDN (Brazil).

Preparation and Characterization of Samples. The semicontinuous emulsion copolymerization process was carried out in a 250 mL reactor equipped with a mechanical stirrer with a Teflon blade, a thermometer, and a reflux condenser. The reactor was initially loaded with deionized water (60 mL), surfactant SDS (0.11 g), initiator KPS (0.06 g), and pH buffer ($NaHCO_3$, 0.06 g). Two addition funnels, one containing the monomer mixture (a mixture of the monomers nBMA, 33 mL, STY, 5.5 mL and 9-Van, 0.012 g) and another with an aqueous solution prepared with deionized water (20 mL, SDS, 0.60 g and KPS, 0.06 g) were continuously fed under agitation of 300 rpm over a total time interval of 5 h under an atmosphere of argon at 80 °C. The conversion of the monomers (>96%) was evaluated by gravimetry.

The copolymer was precipitated with methanol, then it was washed with methanol to remove unreacted monomer and surfactant, and subsequently, it was washed with water to remove other water-soluble impurities. Finally, it was dried to constant weight in a vacuum oven at 60 °C.

The FTIR spectrum of the copolymer was recorded on a Bomem MB-series model B-100 infrared spectrophotometer by casting thin films of the copolymer from a chloroform solution over a KBr window. The recorded spectra resulted from 4 scans/min with 4 cm^{-1} of resolution.

The high-resolution ^1H NMR spectrum of copolymer was recorded using a Bruker AC300/P, 300-MHz FT-NMR spectrometer, using $CDCl_3$ as solvent and tetramethylsilane as internal standard.

The molar contents of the monomeric units in the copolymer were determined using a Hewlett-Packard-8452A UV−vis spectrophotometer. The molar absorption coefficients $\epsilon_{207} = 69$ L mol^{-1} cm^{-1} (ethyl acetate), $\epsilon_{262} = 260$ L mol^{-1} cm^{-1} (toluene), and $\epsilon_{386} = 9700$ L mol^{-1} cm^{-1} (9-methylanthracene) were employed to determine the relative amount of acrylate groups, styrene, and anthryl groups in the copolymer, respectively.

TABLE 1: Some Physical Properties of NBMAS and PS Polymers

polymer	T_g (°C)	$10^{-3}\bar{M}_n$[a]	$\bar{M}_w/\bar{M}_n$	nBMA (mol %)[b]	STY (mol %)[b]	9-Van (mol %)[b]
nBMAS	22	31.2	2.74	77.5	22.4	0.1
PS	91	64.6	2.58		100	

[a] From GPC. [b] From UV−vis.

Molecular weight and molecular weight distributions of the copolymer and polystyrene were evaluated by gel permeation chromatography (GPC), using a Linear μStyragel column (American Polymer Standards Co.) at 40 °C coupled to a refractive index detector (Waters 410), with THF as the eluent. Monodisperse polystyrene standards were used as the calibration standards. Values for the molecular weights and for polydispersities of these two polymers are depicted in Table 1.

Films of nBMAS/PS blends (approximate thickness of 0.3 mm) were prepared by casting 10% chloroform solutions containing different compositions of each polymer: 5/95, 20/80, 50/50, 80/20, and 95/5 wt % of nBMAS/PS. The solvent was slowly evaporated (2 days at room temperature), and then the films were dried for a day in an oven at 50 °C under dynamic vacuum. They were annealed at 100 °C under dynamic vacuum in an oven for 12 h to minimize the thermal stress and erase prior thermal histories.

The glass transitions of these films were determined by differential scanning calorimetry in a model v2.2A 90, DSC from DuPont, calibrated with indium as standard. The thermograms were scanned at a scan rate of 10 °C min^{-1} and the T_g values were taken as half of the transition (the change of the specific heat) in the DSC thermograms.

Epifluorescence microscopy was performed using a Leica DM IRB inverted fluorescence microscope employing objectives with optical magnification values of 6.3×, 12.5×, and 25×. For EFIM measurements, a 100 W Hg arc lamp was employed for excitation, with its wavelength range of 330−380 nm selected by optical filters. The emission image was separated from the excitation beam by a dichroic mirror ($\lambda_{exc} > 410$ nm). Photomicrographs were obtained using two microscopy configurations: epifluorescence optical microscopy (EFIM) and epifluorescence combined with conventional transmission optical microscopy (EFIM/TOM) to improve the image contrast. Epifluorescence images of nBMAS/PS blends were visualized in the micrographs by the blue regions (fluorescence from anthryl labeled copolymer nBMAS) and the completely dark regions (PS), because any possible emission from PS regions is completely cut off by the dichroic mirror.

Steady-state fluorescence spectroscopy was performed using an ISS−PC1 spectrofluorimeter with an excitation wavelength of $\lambda_{exc} = 262$ nm and the fluorescence emission collected from 270 to 500 nm. Excitation spectra were collected from 340 to 410 nm, with $\lambda_{em} = 420$ nm.

Fluorescence decays were obtained with a time-resolved FL 900 spectrofluorimeter (Edinburgh Analytical Instruments, Edinburgh, U.K.), using the time correlated single photon counting (TCSPC) method. Excitation of the samples was carried out by a pulsed hydrogen flash-lamp controlled by a Thyratron tube operating with a repetition frequency rate of 40 kHz. The sample in the cuvette was evacuated for 15 min, and then the cuvette

was sealed. Measurements were performed with exciting irradiation at 262 nm and the emission was collected at both wavelengths: at $\lambda_{em} = 340$ nm (for the emission from the excimer phenyl groups) and at $\lambda_{em} = 420$ nm (for the emission from the anthryl groups). All measurements were performed at room temperature.

The observed decays of fluorescence intensity $R(t)$, is given by the convolution integral:

$$R(t) = \int_0^t F(t-t')\, L(t')\, dt \quad (1)$$

where $L(t)$ is the time distribution of the lamp pulse and $F(t)$ is the (theoretical) response function corresponding to a infinitely short excitation lamp pulse. $L(t)$ was measured using a solution of LUDOX (DuPont) closely spaced in time to particular fluorescence decay experiments. The data were analyzed by the exponential series method (ESM) described elsewhere,[27] which assumes that the fluorescence decay, $F(t)$, can be analyzed as a multiple exponential function as

$$F(t) = \sum_{i=1}^{N} A_i \exp(-t/\tau_i) \quad (2)$$

where A_i is a preexponential factor representing the fractional contribution to the time-resolved decay of the component with a lifetime τ_i and t is the time. The ESM considers eq 2 as a discrete approximation to

$$F(t) = \int_0^\infty A(\tau) \exp(-t/\tau)\, d\tau \quad (3)$$

and uses $N > 20$ for the fixed lifetime values. Here $A(\tau)$ is the continuous fluorescence lifetime distribution causing the observed decay. Thus, the preexponential values recovered from the fit represent an approximation to $A(\tau)$. The ESM uses a fixed set of lifetimes and fits to freely adjustable A_i values that are constrained to be positive. The search for the best fit uses the "Marquardt algorithm" to minimize the reduced χ^2 (goodness of fit). If, during the iterative minimization process, a preexponential value falls below 1% of the current maximal A_i, that preexponential value is fixed at zero to facilitate convergence.

Results and Discussion

Polymer Characterization. The nBMAS-copolymer FTIR spectra (not shown) exhibit several IR-bands characteristic of the acrylate segments, such as antisymmetric stretching vibrations of the CH_3 groups (2985−2994 cm^{-1}), symmetric stretching vibrations of the CH_3 groups (2952−2862 cm^{-1}) overlapped with the stretching vibrations of the CH_2 groups (2845−2852 cm^{-1}), C═O stretching vibrations (1730−1720 cm^{-1}), bending vibrations of CH_3 and CH_2 groups (1451−1443 cm^{-1}), and rocking vibrations of CH_2 (757−755 cm^{-1}). The IR spectrum also shows the characteristic absorption bands of the phenyl ring belonging to the styrene block, such as −C═C− stretching vibrations (1591−1604 cm^{-1}), C−H bending (730−770 cm^{-1}), and aromatic −C−H stretchings (3000−3100 cm^{-1}).

The proton NMR spectrum of the copolymer shows chemical shifts for the phenyl groups of the styrene blocks (6.92−7.24 and 3.06−3.10 ppm) and the oxymethylene groups (OCH_2) (3.58−3.87 ppm) and methylene groups (1.23−1.91 ppm) of the nBMA units in the copolymer. The resonance peaks from the methyl groups in the copolymer appear in the 0.51−0.87 ppm region.

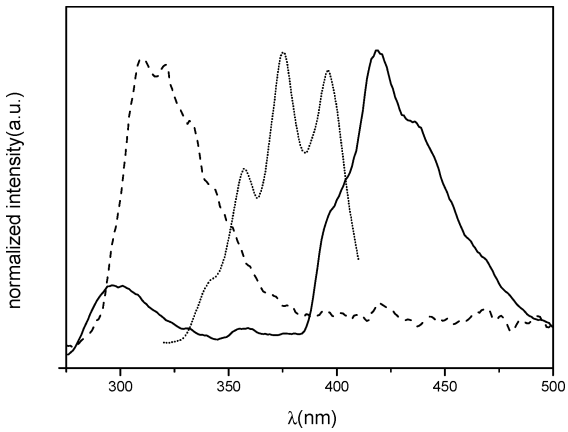

Figure 1. Fluorescence spectra of nBMA (—) and PS (- - -) (λ_{exc} = 262 nm) and excitation spectra of nBMA (···) (λ_{em} = 420 nm), in the solid state.

The glass transition temperature (T_g) of both nBMAS (trace 1 in Figure 3) and PS (trace 7 in Figure 3), determined by DSC, were 22 and 91 °C, respectively (Table 1). Because the T_g of the two neat components (nBMA and PS) are very different and are relatively sharp, the broadening can be used as a criterion for molecular intermixing in their polymer blends.

On the basis of the UV/vis absorption spectrum of the copolymer and on the molar absorptivity coefficients, we calculate the relative amount of each block in the copolymer as shown in Scheme 1 and in Table 1.

Photophysical Behavior of the Polymers. In Figure 1 we show the fluorescence spectrum of the PS homopolymer, which is characterized by a broad and partially structured emission band with a peak at 310 nm. This band is assigned to the emission of both preformed dimers and of excimers involving the phenyl groups.[28] The emission band of the copolymer is composed of two components: the higher energy band centered at ∼296 nm is attributed to isolated phenyl groups of the styrene blocks. The second emission, with a peak at ∼420 nm, is attributed to the anthryl groups randomly copolymerized to both styrene and acrylic segments in the copolymer. This figure also shows the excitation spectra of the anthryl groups, whose vibronic profile is similar to those of several other anthracene derivatives.[29] In Figure 1 we observe a partial overlap of the emission band of the PS excimers with the excitation band of the anthryl groups, which, in principle, allows the energy transfer process between these groups, depending on their distance. In addition, the fluorescence band of the anthryl groups is broader than usual due to a broad distribution of polymer chain conformations.[30]

Figure 2 shows the decay profile of the excimer-like emission of PS and of the styrene blocks of the nBMAS copolymer (λ_{exc} = 262 nm and λ_{em} = 340 nm). The decay profile of the PS excimer (Figure 2a) was fitted to a biexponential function with a faster ($\langle\tau\rangle = 3.7 \pm 1.0$ ns) and a slower ($\langle\tau\rangle = 21.0 \pm 4.7$ ns) components. The slower component matches the usual excimer lifetime of phenyl groups in PS,[31] whereas the faster component may be assigned to the singlet−singlet annihilation process of the same excimer group.[32] The decay profile of the excimer phenyl groups in nBMAS copolymer (Figure 2b) was also fitted by a biexponential function and two average lifetimes were obtained: $\langle\tau\rangle = 11.3 \pm 0.9$ ns and $\langle\tau\rangle = 3.0 \pm 0.3$ ns, which were again attributed to the normal and the S_1-S_1 annihilation emissions, respectively. In contrast with PS and its model compounds, the excimer-like emission of phenyl groups or other aromatic moieties in copolymers exhibits a more complex

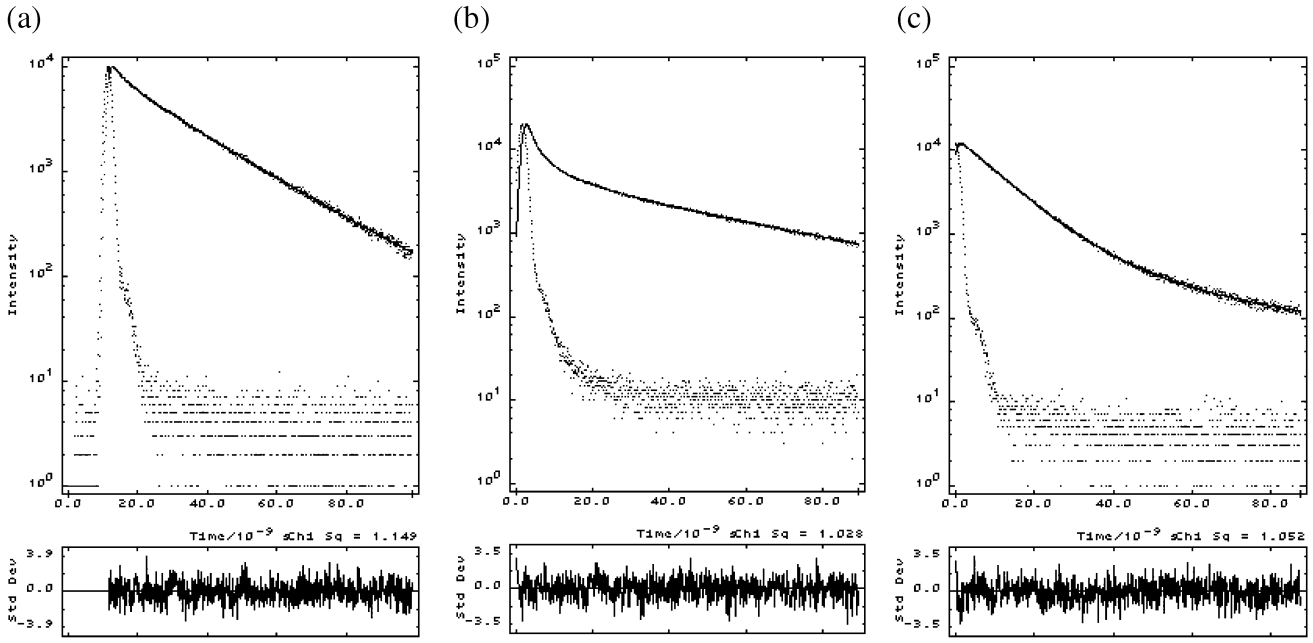

Figure 2. Fluorescence decays collected at $\lambda_{em} = 340$ nm for (a) polystyrene and (b) nBMAS copolymer and (c) at $\lambda_{em} = 420$ nm for the anthryl groups. $\lambda_{exc} = 262$ nm.

photophysical behavior upon excitation of the aromatic moieties.[33,34] If the distance between the phenyl moieties is large, they behave as isolated chromophores and emission from isolated groups is obtained. This is the case of copolymers with longer acrylate spacers.[32] Nevertheless, in present systems, we are observing excimer-like emission, suggesting the existence of randomly distributed blocks of styrene segments.

Figure 2c shows the decay profile of the emission from the anthryl groups in nBMAS copolymer. The experimental data were fitted by a monoexponential function with a very narrow lifetime distribution having an average lifetime of $\langle\tau\rangle = 10.2 \pm 0.7$ ns, which is in agreement with values expected for anthracene derivatives.[35] Because the sample is excited at $\lambda_{exc} = 262$ nm, where the most important absorption is attributed to the phenyl moieties, we are assuming that the energy transfer process from the excimer-like phenyl moieties to the anthryl groups is the most important mechanism. Nevertheless, two mechanisms for the energy transfer could take place: (i) energy transfer from the phenyl to the anthryl groups by the Förster mechanism; (ii) energy transfer from the phenyl to the anthryl groups by a trivial process. These processes depend differently on the interlumophoric distance and on the relative orientation of the donor and acceptor groups[36] and could not be distinguished in the present work.

Thermal Properties and Morphology of nBMAS/PS Blends. All thermograms (Figure 3) are the results of the second run after heating the sample to 150 °C (which is above the glass transition temperature) to erase the thermal history of each sample, quenching it to −100 °C (cooling rate of 20 °C/min), and heating again to 150 °C (heating rate of 10 °C/min). The trend of T_g versus composition plot is analyzed together with the morphology determined by EFIM. Figure 4a shows the EFIM micrograph of the blend with 95% PS. It seems a uniform system, with interconnected zones with more intense fluorescence, better visualized when we combine epifluorescence with auxiliary transmission white light (EFIM/TOM). For this sample we cannot identify nonfluorescent zones and the emission is very diffuse and distributed throughout the entire sample. The DSC measurement gives a single T_g (64 °C) value (trace 6 in Figure 3), which is significantly lower than the glass transition temperature of PS, ca. 93 °C (trace 7 in Figure 3). Both data, within the limit of their spatial resolution, suggest that the blend with this composition forms a miscible system.

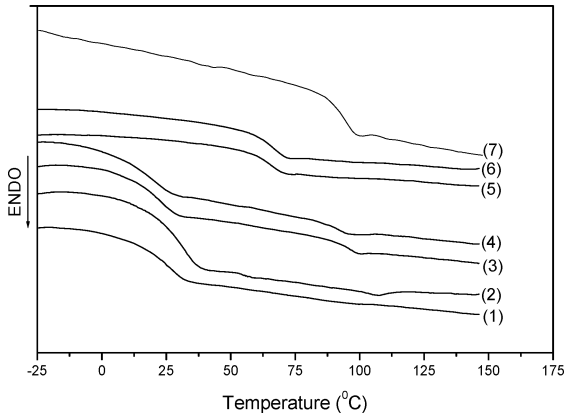

Figure 3. DSC traces (second run) of nBMAS (1); blends of nBMAS/PS with 5% (2), 20% (3), 50% (4), 80% (5), and 95% w/w (6) in PS; and PS (7).

In micrograph Figure 4b, for blends with 80% PS, we observe interconnected small droplets of strongly fluorescent material distributed over weaker fluorescent zones that are surrounded by an interconnected nonfluorescent (dark) matrix. Interconnected regions are characteristic of morphologies produced by a phase separation process known as spinodal decomposition.[1] Again the DSC trace (trace 5 in Figure 3) shows a single T_g (63 °C) value. Although total miscibility is suggested by these data, the micrograph suggests a partial phase separation. Earlier reports in the literature[37,38] discussed similar results, where blends with a single value of T_g in the DSC thermograms are not necessarily forming a completely miscible system. Indeed, these data suggest miscibility under a certain limit of the size of the separated phases. Thus, we are assuming that the single value of T_g results in a great extent to the miscible part of the material and the immiscible part is segregated in form of cocontinuous phases.

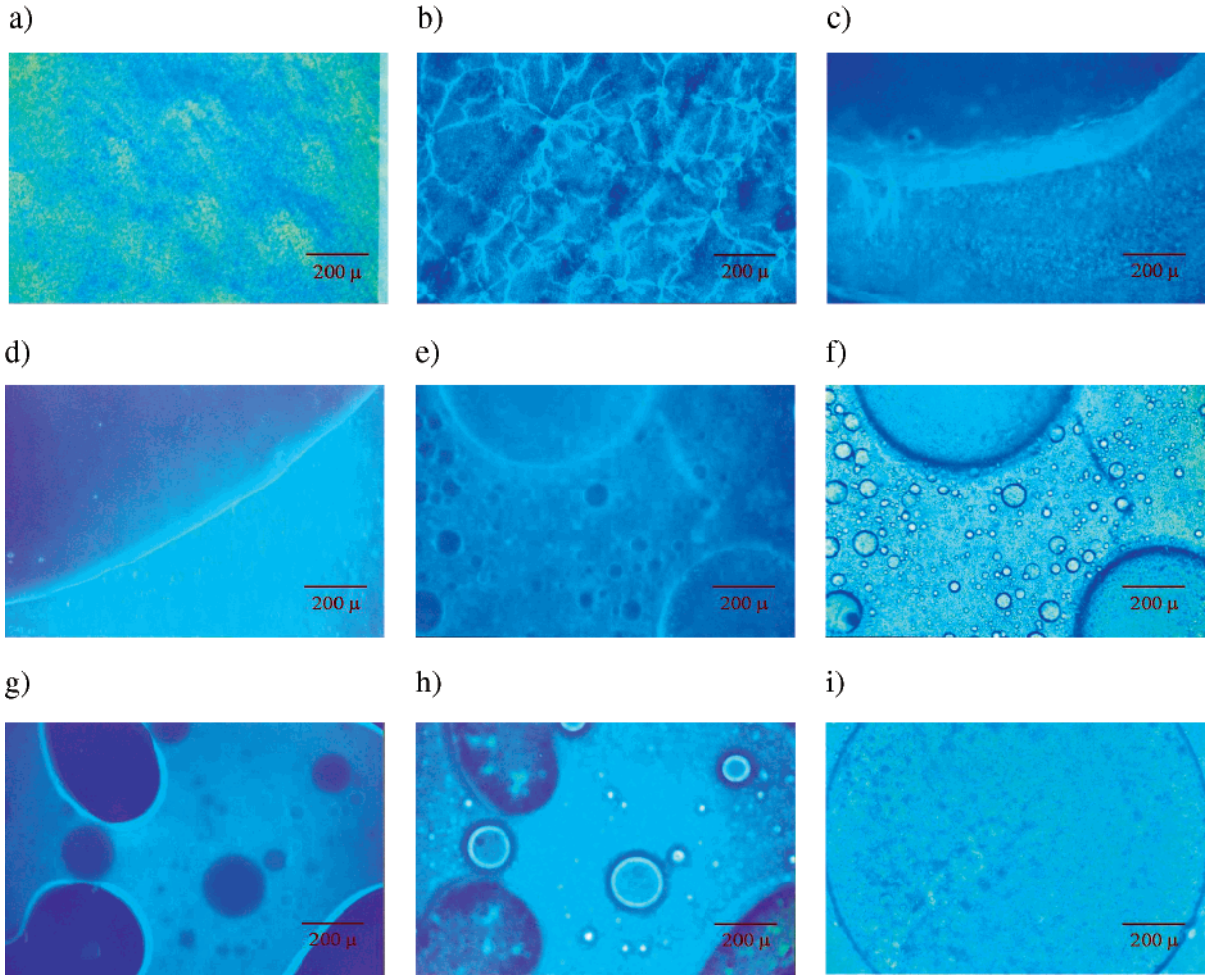

Figure 4. Micrographs of chloroform-cast nBMAS/PS blend samples: (a) EFIM of 5/95; (b) EFIM of 20/80; (c) and (d) EFIM of 50/50 nonannealed and annealed blends, respectively; (e) and (f) EFIM and EFIM/TOM of 80/20 nonannealed blend, respectively; (g) and (h) EFIM and EFIM/TOM of 80/20 annealed blend, respectively, and (i) EFIM/TOM image of 95/5.

Differently, blends with 50% PS exhibit well-defined nonfluorescent spherical droplets dispersed in a fluorescent matrix. Moreover, in nonannealed samples (Figure 4c) there is a broad and strongly fluorescence interface that becomes sharper in the annealed material (Figure 4d). Polymer blends with spherical droplets dispersed in a matrix are usually produced by a mechanism known as nucleation and growth.[1,2] The DSC thermograms (trace 4 in Figure 3) show two broadened glass transitions (13 and 91 °C), in agreement with a biphasic system. These suggest that the droplets are composed of PS whereas some miscibility takes place in the matrix.

The micrographs in Figure 4e,f for nonannealed 80/20 nBMAS/PS blend reproduces the results with 50% PS, showing several nonfluorescent spherical droplets with a broad distribution of sizes dispersed in a fluorescent matrix. Again, phase separation by nucleation and growth is the mechanism that defines this morphology. Coalescence of low fluorescent domains produced by annealing of the samples is responsible for the enrichment of the PS composition inside the domains (Figure 4g,h), which become completely nonfluorescent. Furthermore, the thermally equilibrated morphology after annealing leads to a more complete phase separation and to well-defined (sharper) interfaces. Two T_g values (20 and 94 °C) from DSC (trace 3 in Figure 3) with sharper profiles of the DSC traces are observed. These values are similar to those of the neat components (traces 1 and 7 in Figure 3).

The morphology of the blend with 95% nBMAS is shown in Figure 4i. A biphasic nonuniform material that contains several large fluorescent droplets (copolymer richer parts) with occlusion of smaller nonfluorescent droplets (PS richer parts) is observed. This type of morphology results from a sequence of phase separation processes: a first step producing a large gelified phase followed by a secondary phase separation of a PS phase inside the large copolymer droplets. The glass transitions observed are 19 °C (copolymer richer-phase) (trace 2 in Figure 3), 98 °C (PS phase), and a middle value at 49 °C, which demonstrate partial miscibility in this system.

Figure 5 shows the influence of the composition dependence on the morphology for blends with several compositions. This scheme is an attempt to describe the relationship between T_g and composition for the nBMAS/PS blends. We also include a cartoon depicting the mechanisms of phase separation for every composition range, from the miscible blends (nBMAS content < 20%) with the spinodal phase separation (at lower nBMAS contents), for immiscible blends with prevalence of the dispersed droplets in a matrix produced by the nucleation and growth mechanism (at higher nBMAS content), and for blends where the primary and secondary phase separation processes by nucleation and growth mechanism take place (at very high nBMAS content).

Local Morphology in nBMAS/PS Blends. Data shown in the previous sections indicated that blends of nBMAS/PS should be miscible depending on the composition. Nevertheless, these

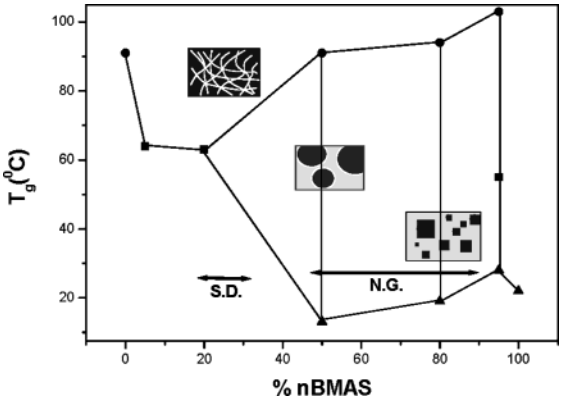

Figure 5. Scheme with the values of T_g for nBMAS/PS blends with several wt % contents of nBMAS. The cartoons illustrate the mechanisms of phase separation. S.D. = spinodal decomposition, N.G. = nucleation and growth.

data are based on low spatial resolution; optical microscopy can identify domains with sizes of a few micrometers and DSC can identify glass transitions of domains in the same spatial resolution. Differently, nonradiative energy transfer processes involving donor/acceptor groups occur in the spatial range of a few nanometers. In this section the miscibility will be evaluated from the decay of the fluorescence emission from the donor (phenyl excimer-like groups) in the presence of the acceptor (anthryl moieties) if they are separated by only a few nanometers (Förster radius). Thus, it is a measurement of the phase interpenetration at the molecular level, which can reasonably indicate local miscibility or local morphology.

It has been established that the lifetime for donor fluorescence decreases in the presence of an acceptor, according to the Förster theory for nonradiative energy transfer processes:

$$\frac{\tau_D}{\tau_{DA}} = 1 + \left(\frac{R_0}{r}\right)^6 \tag{4}$$

where τ_D and τ_{DA} are the fluorescence lifetimes for the donor groups in the absence and presence of the acceptor, respectively, r is the distance between donor and the acceptor groups, R_0 is the characteristic distance for each specific donor/acceptor pair (1.54 nm, according to a reference value[39] for donor polystyrene, acceptor 9-methylanthracene) and it is given by

$$R_0^6 = \frac{9.000k^2Q_D \ln 10}{128\pi^5 n^4 N_A}\int\frac{F_D(\tilde{\nu})\,\epsilon_A(\tilde{\nu})}{\tilde{\nu}^4}\,d\tilde{\nu} \tag{5}$$

where $\tilde{\nu}$ is the wavenumber, $\epsilon_A(\tilde{\nu})$ is the molar extinction coefficient of the energy acceptor, $F_D(\tilde{\nu})$ is the normalized fluorescence spectral distribution of the excitation donor, Q_D is the fluorescence quantum yield of the energy donor, N_A is Avogrado's number, n is the refractive index of the blend, and k^2 is an orientation factor, which in the case of random directional distribution is $^2/_3$. According to eq 4, a decrease of the lifetime is expected for distances lower than the Förster radius. Upon closer examination of eq 5, the efficiency of the NRET process is also dependent on the spectral overlap between the donor emission and the acceptor absorption, which is remarkable, as shown in Figure 1. From this figure we can see that the overlap between the emission from the isolated phenyl groups and the absorption of anthryl is very small and, consequently, the most important energy transfer process will involve the polystyrene and the copolymer instead of the styryl moieties of the copolymer.

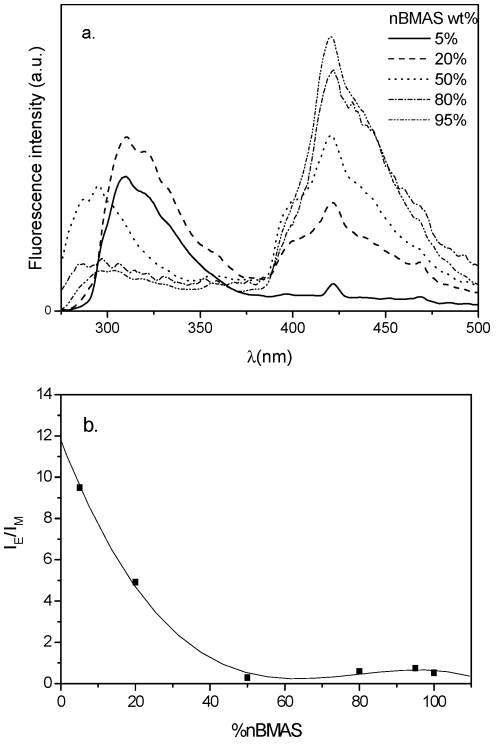

Figure 6. (a) Emission spectra of chloroform-cast nBMAS/PS blend with several copolymer compositions (λ_{exc} = 262 nm). (b) I_E/I_M ratio for the same blends. I_E and I_M are intensity at 340 and at 280 nm, respectively.

In the present work we measured the decay of the fluorescence emission from both the phenyl excimer groups in PS (which represents the emission in the absence of the acceptor) and in the blends with nBMAS (which represent the emission in the presence of the acceptor groups using λ_{exc} = 262 nm). The data are analyzed on the basis of the distribution analysis of the fluorescence lifetime. Distribution analysis for the fluorescence lifetime was chosen because the fit of the experimental data using sum of discrete requires at least three (in some cases more) exponential functions for an acceptable fit. Moreover, no systematic correlation between the lifetime values and the morphology of the blends should be obtained. On the other hand, although distribution analysis introduces many adjustable parameters, it is more representative for the microheterogeneity and for the complexity of the morphology of polymer blends. As we will show, there is a systematic correlation between the average fluorescence lifetimes and the morphology determined by epifluorescence as well as with the glass transition temperature values determined by DSC. For example, sharper distribution of lifetimes is obtained for blends with lower miscibility (larger amount of the copolymer).

Figure 6a shows the fluorescence spectra (λ_{exc} = 262 nm) for nBMAS/PS blends with several compositions. Two bands with the relative intensity dependent on the composition were observed: (i) the emission from 275 to 350 nm, attributed to the phenyl groups, and (ii) the emission from 390 to 490 nm, attributed to the anthryl moieties from the copolymer. The spectral profile of the higher energy band changes with the composition: the band centered in 310 nm is like that in the PS spectrum (Figure 1) and appears in the PS-richer samples (80% and 95%). That centered at 296 nm is like that in the nBMAS spectrum (Figure 1) and appears in the symmetrical (50%) to the nBMAS-richer compositions (80% and 95%). It is attributed to the isolated phenyl groups. Nevertheless, the

fluorescence bands of excimeric-like phenyls are always overlapped with the absorption band of anthryl (shown in Figure 1).

Figure 6b exhibits the results of the intensity ratio for the excimer/monomer, I_E/I_M, in nBMAS/PS blends as a function of the nBMAS composition, determined by steady-state fluorescence spectroscopy, where I_E is the intensity of the fluorescence of the excimer, $\lambda_{em} = 310$ nm, and I_M is the intensity of fluorescence of the isolated chromophore, $\lambda_{em} = 296$ nm. This ratio decreases with the increase of nBMAS content from 5 to 50 wt % and finally becomes virtually constant for compositions 50%, 80%, and 95%. The values of this ratio result from the contributions coming from the PS homopolymer in the blend and from the PS blocks in the copolymer. It is noteworthy that the excimer and monomer intensity ratio does not scale linearly with the fraction of PS. For example, excimer emission of the blend with 50% PS is less 5%, which should not be expected unless this phase is disturbed by the copolymer. In addition, we should expect that the excimer-like emission will be more important for higher concentrations of phenyl groups in a specific phase and in systems where the PS-block acquires folded conformations. On the other hand, the lower values of I_E/I_M reflect the more extended chain in the system with a partial miscibility between the components or systems where the phenyl moieties are separated by acrylic blocks and thus cannot achieve the folded conformation required for the excimer-like structure (Figure 4a−d). Thus, we consider that this ratio reflects to some extent the coil organization of the styrene blocks in the blends.

Figures 7 and 8 illustrate the distribution of fluorescence lifetimes based on the ESM method for blends with several compositions. As shown, a multiexponential decay was constructed, convoluted with the instrument response function (IRF), and submitted to ESM analysis. Table 2 shows that the average lifetime for the excimer phenyl moieties is shorter ($\langle\tau\rangle = 17.8 \pm 5.6$ ns) for the 05/95 nBMAS/PS blend, in relation to the PS excimer ($\langle\tau\rangle = 21.0 \pm 4.7$ ns). Shorter lifetimes should be explained by intermolecular energy transfer process from excimers to traps inside the PS blocks or to the anthryl groups located in the copolymer chain both within the Förster radius. On the other hand, we are assuming that a broader distribution of the lifetimes, observed for miscible blends or for those blends with interconnected phases, results from a broader distribution of distances separating donors and acceptors involved with the Förster energy transfer process. In addition, we also observed a broader lifetime distribution (Figure 7b) that could be related to the microheterogeneity of the system composed by interconnected PS and nBMAS phases (Figure 4a).

According to the Förster nonradiative energy transfer process, the decrease of the fluorescence lifetime from the donor in the presence of the acceptor requires that the average distance between these groups is similar to the Förster radius, ca. 1.54 nm. Because the energy transfer is occurring between the PS and nBMAS chains, it also requires interpenetration of both phases that explains the observed morphology and the miscibility detected by DSC (a single T_g value).

Figure 7c shows the fluorescence lifetime distribution of the excimer phenyl groups for the blend with 80% PS, which exhibits a cocontinuous morphology (Figure 4b). For this composition we also observed a broad distribution for the average decays at $\lambda_{em} = 340$ nm ($\langle\tau\rangle = 20.0 \pm 6.4$ and 3.2 ± 1.4 ns). The interpretation for the shorter lifetimes compared to neat PS is the same as previously described and requires phase interpenetration or, at least, a partial miscibility, in agreement with a single T_g value determined by DSC.

A bimodal lifetime distribution of the excimer phenyl groups for the blend with symmetric composition (Figure 7d) was determined, where the average lifetimes for longer decay ($\langle\tau\rangle = 21.8 \pm 10.9$ ns) and annihilation singlet−singlet ($\langle\tau\rangle = 3.2 \pm 0.9$ ns) exhibited similar amplitudes. Moreover, the distribution of the longer decays is much broader, revealing heterogeneity and large distribution of distances among donors and acceptors in the system, in agreement with the complexity of the morphology as shown in Figure 4c. The morphology of these blends can be characterized by three types of distinct domains: one composed of PS, a second composed of the copolymer, and the third, where a partial miscibility is observed, probably involves those broad interphases, where some NRET takes place.

In contrast, for nBMAS-richer compositions the lifetime distributions for both decays are narrower for both blends (80/20 and 95/05 nBMAS/PS) (Figure 7d,e) as observed for the neat copolymer (Figure 7f). For these systems a faster excimer average lifetime ($\langle\tau\rangle = 13 \pm 1.3$ ns) takes place. As discussed earlier, the probability of the energy transfer process is strongly dependent on the overlap between the fluorescence emission from the donor (Figure 6) and the absorption spectra from the acceptor (Figure 1). This overlap is very small for blends with compositions of 20 and 5% PS, as well as for the copolymer. Thus, the faster decay rate (similar to the copolymer 11.3 ± 0.9 ns) should more probably be explained by the more important changes of the microenvironmental properties (interchain proximity of the phenyl and the acrylic moieties and polarity of the medium) than by polymer miscibility and interpenetration of the PS and nBMAS chains. Indeed, phase separation and low miscibility is evident from the fluorescence micrographs (Figure 4e−i) and from the glass transition values recorded by DSC (Table 2).

Parts a−f of Figure 8 show the fluorescence lifetime distribution of the anthryl group acceptor for the blends of nBMAS/PS and for the nBMAS copolymer. For the copolymer (Figure 8f) the lifetime distribution is narrow and, therefore, they can be well represented by a monoexponential decay with a discrete value of 10.0 ± 1.0 ns (Table 2). The broadening of the distribution, represented by the increase of standard deviation value, from neat copolymer toward the PS-richer blends is clearly seen. Again, broad distribution of lifetimes is observed for blends with partial miscibility (20% and 50% copolymer, Figure 4b,c) or with larger interconnected zones (5% copolymer, Figure 4a). A broader distribution suggests that several types of microenvironments surround the anthryl groups.

In addition, Figure 6a shows that the self-absorption process from the anthryl moieties appears in blends with 80% and 95% nBMAS, for which there is a remarkable decrease (or disappearance) of the relative intensity of the 0−0 vibronic band. Self-absorption and re-emission are types of energy transfer processes that increase the fluoroprobe emission lifetimes, according to

$$\tau_F = \frac{\tau_F^0}{1 - aq_{FM}} \tag{6}$$

where $a = 2.313[M](d/q_{FM})\int F(\bar{\nu})\,\epsilon(\bar{\nu})\,d(\bar{\nu})$, [M] is the concentration, $\epsilon(\bar{\nu})$ is the molar extinction coefficient at frequency ν, d is the sample thickness, and q_{FM} is the fluorescence quantum yield in the absence of trivial energy transfer process. This is a very efficient process for anthracene molecules and anthryl groups because of the strong overlap (small Stoke's shift)

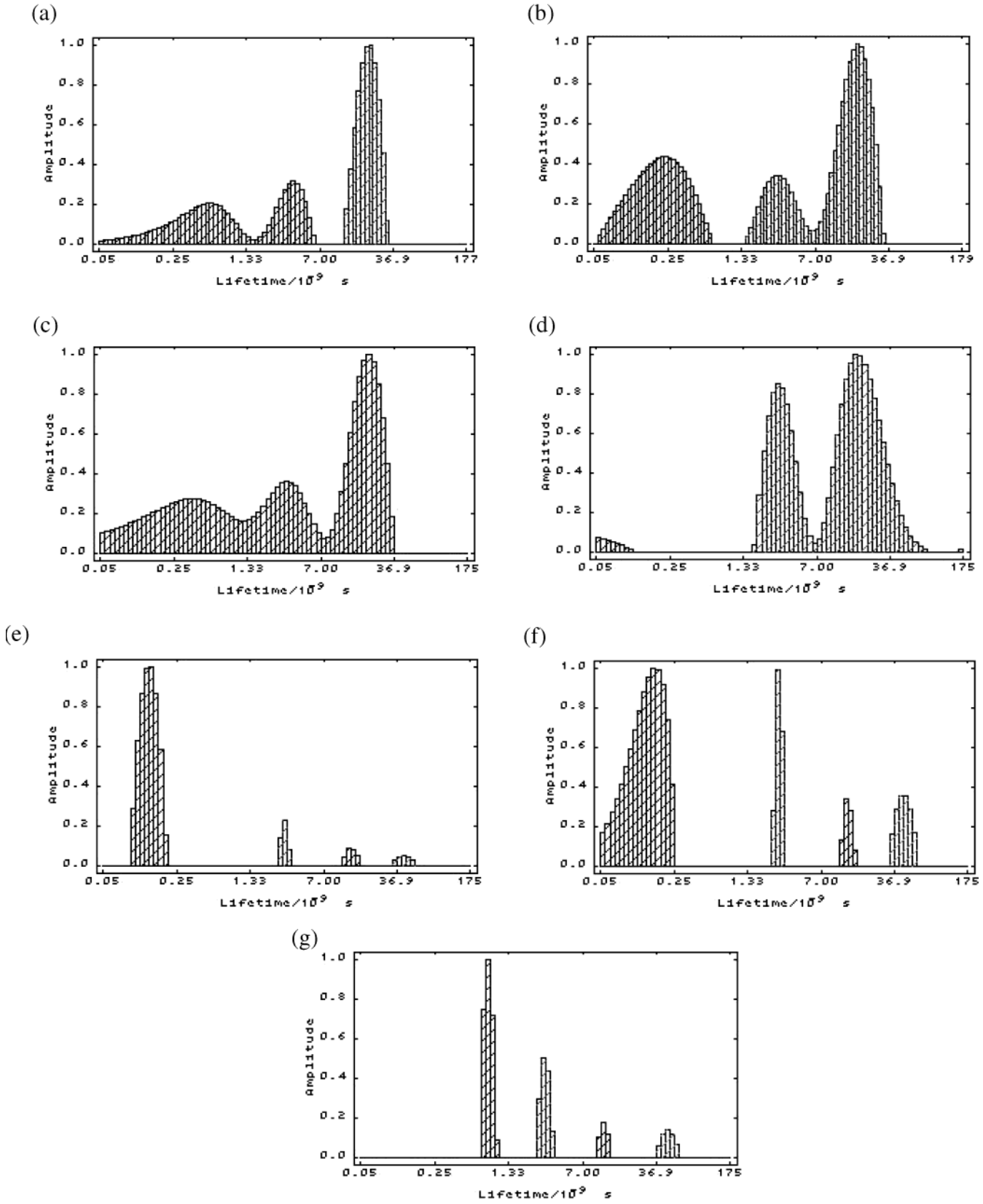

Figure 7. Fluorescence lifetime distribution of phenyl excimers ($\lambda_{exc} = 262$ nm, $\lambda_{em} = 340$ nm) of (a) PS, (b) 05/95, (c) 20/80, (d) 50/50, (e) 80/20, (f) 95/05 nBMAS/PS (wt %) blends, and (g) nBMAS copolymer. The decay curves were collected in 1024 channels and analyzed with the ESM method.

between their excitation (absorption) band and fluorescence emission (see Figure 1), which are also strongly dependent on the concentration. Therefore, when we increase the relative amount of nBMAS in the blends, self-absorption processes (a property of the anthryl groups themselves) can occur simultaneously with the NRET from excimer phenyl groups to anthryl groups (an interchain process) and there is an increase of the fluorescence lifetime as observed for blends with 80% and 95% copolymer and neat copolymer ($\langle\tau\rangle = 9.3 \pm 1.5$ ns to $\langle\tau\rangle = 10.0 \pm 1.0$ ns, respectively) (Table 2).

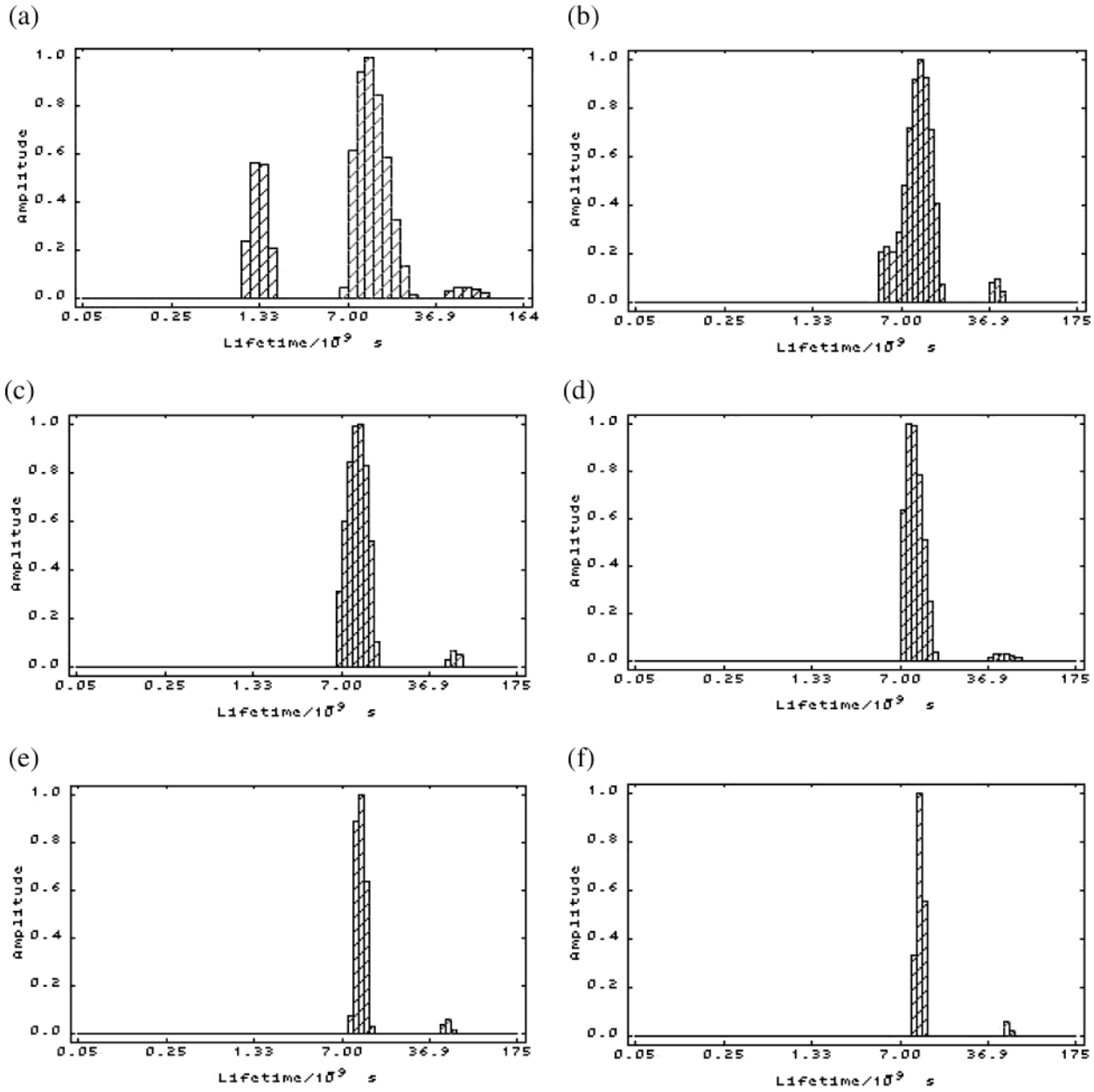

Figure 8. Fluorescence lifetime distribution of anthryl groups ($\lambda_{exc} = 262$ nm, $\lambda_{em} = 420$ nm) on nBMAS/PS (wt %) blends: (a) 05/95; (b) 20/80; (c) 50/50; (d) 80/20; (e) 95/05; (f) nBMAS copolymer. The decay curves were collected in 1024 channels and analyzed by the ESM method.

TABLE 2: Glass Transition Temperatures and Fluorescence Lifetimes for the NBMAS/PS Blends and the Neat Components

		$\lambda_{em} = 340$ nm			$\lambda_{em} = 420$ nm		
nBMAS content (wt %)	T_g(°C)	$\langle\tau\rangle$(ns)	std dev	χ^2	$\langle\tau\rangle$(ns)	std dev	χ^2
0	91	3.7	1.1	1.15			
		21.0	4.7				
5	64	3.2	1.1	1.08	11.5	3.4	1.08
		17.8	5.6				
20	63	3.2	1.4	1.03	9.9	2.2	1.16
		20.0	6.4				
50	13	3.2	0.9	1.13	9.5	1.8	1.16
	91	21.8	10.9				
80	20	2.8	0.2	1.17	9.3	1.5	1.19
	94	13.2	1.4				
95	19	2.7	0.2	1.09	10.0	1.0	1.05
	49	13.0	1.2				
100	22	3.0	0.3	1.03	10.0	1.0	1.05
		11.3	0.9				

Conclusions

Blends of nBMAS with PS were studied in several compositions (5−95% in PS). For compositions with PS > 80% w/w, we observed broader distribution of the fluorescence lifetimes for both decays (from excimer-like and from anthryl moieties), higher I_E/I_M ratios, a co-continuous morphology with interconnected domains from epifluorescence microscopy, a single T_g in DSC thermograms, and lower efficiency of the trivial energy transfer processes for the anthryl groups. All these data together confirm that we have a miscible system where interpenetration of both PS and copolymer chains takes place, which cannot be reached for homopolymer PMMA and PS blends. For blends with nBMAS up to 80% we observe phase separation characteristic of a primary nucleation−growth mechanism. The ESM methodology applied to the decay of the fluorescence emission showed a drastic narrowing of the lifetime distribution, the epifluorescence micrographs show nonfluorescent spherical domains dispersed over the entire fluorescent matrix, with a wide distribution of sizes. Two values of glass transitions are observed and, from the analysis of these data, we conclude that we have immiscible blends. Blends with 95% copolymer also show phase separation, produced by sequential nucleation−

growth processes. Primarily, large droplets are produced and then a secondary phase separation process takes place inside the droplets. Epifluorescence microscopy is a very convenient technique for observing such kinds of secondary processes. Steady-state fluorescence spectroscopy and time-resolved fluorescence spectroscopy are in agreement with the morphology determined by epifluorescence microscopy and with the DSC data, allowing discussion of miscibility in nanoscale domains.

We also observed, by epifluorescence microscopy, that the annealing process introduced two types of changes in the material prepared by casting: (i) enhancement of the phase separation in those systems presenting secondary phase separation by nucleation and growth; (ii) reduction of the thickness of the interface.

Acknowledgment. T.D.Z.A. thanks FAPESP and MCT/PADCT/IMMP for financial support. T.D.Z.A. and M.L.A. acknowledge fellowships from CNPq. We thank M. R. Pinto for discussions during the copolymer synthesis. We also thank Prof. Carol Collins for useful discussions.

References and Notes

(1) Paul, D. R., Newman, S., Eds. *Polymer Blends*; Academic Press: New York, 1987.

(2) Utracki, L. A. *Polymer Alloys and Blends: Their Thermodynamics and Rheology*; Carl Hanser: Munich, 1989.

(3) Jiang, M.; Cao, X.; Chen, W.; Yu, T. *Polym. Bull.* **1989**, *21*, 599.

(4) Jiang, M.; Cao, X.; Chen, W.; Yu, T. *Makromol. Chem. Symp.* **1990**, *38*, 161.

(5) Hobbie, E. K.; Han, C. C. *J. Chem. Phys.* **1996**, *105*, 738.

(6) Simmons, A.; Natansohn, A.; Eisenberg, A. *J. Polym. Sci., Polym. Chem.* **1987**, *25*, 2221.

(7) Hack, Th.; Abetz, V.; Stamm, M.; Schubert, D. W.; Mortensen, K.; Siol, W. *Colloid Polym. Sci.* **1996**, *274*, 350.

(8) Merfeld, G. D.; Maa, T. T.; Chan, K.; Paul, D. R. *Polymer* **2000**, *41*, 663.

(9) Edel, V. *Macromolecules* **1995**, *28*, 6219.

(10) Schubert, D. W.; Abetz, V.; Stamm, M.; Hack, T.; Siol, W. *Macromolecules* **1995**, *28*, 2519.

(11) Pellegrini, N. N.; Composto, R. J.; Winey, K. I. *J. Polym. Sci. Part B: Polym. Phys.* **2000**, *38*, 1547.

(12) Braun, D.; Kohl, P. R.; Hellmann, G. P. *Makromol. Chem.* **1988**, *189*, 1671.

(13) Campbell, G. C.; VanderHart, D. L.; Feng, Y.; Han, C. C. *Macromolecules* **1992**, *25*, 2107.

(14) Morawetz, H. *Science* **1979**, *203*, 405.

(15) Amrani, F. J.; Hung, M.; Morawetz, H. *Macromolecules* **1980**, *13*, 649.

(16) Dibbern-Brunelli, D.; Atvars, T. D. Z. *J. Appl. Polym. Sci.* **1995**, *58*, 779.

(17) Serrano, B.; Baselga, J.; Bravo, J.; Mikes, F.; Sese, L.; Esteban, I.; Piérola, I. F. *J. Fluoresc.* **2000**, *10*, 135.

(18) Halary, J. L.; Larbi, F. B. C.; Oudin, P.; Monnerie, L. *Makromol. Chem.* **1988**, *189*, 2117.

(19) Mani, S.; Malone, M. F.; Winter, H. H. *J. Rheol.* **1992**, *36*, 1625.

(20) Semerak, S. N.; Frank, C. W. *Macromolecules* **1981**, *14*, 443.

(21) Semerak, S. N.; Frank, C. W. *Macromolecules* **1984**, *17*, 1148.

(22) Levitz, P., Drake, J., Klafter, J. S. *Molecular Dynamics in Restricted Geometries*; John Wiley & Sons: New York. 1989.

(23) Dong, L.; Hill, D. J. T.; Cai, Y.; Zheng, J. *Polym. Bull.* **1994**, *32*, 347.

(24) Feng, J.; Yekta, A.; Winnik, M. A. *Chem. Phys. Lett.* **1996**, *260*, 296.

(25) Atvars, T. D. Z.; Esteban, I.; Illera, B.; Serrano, B.; Vigil, M. R.; Piérola, I. F. *J. Luminesc.* **1997**, *72*, 467.

(26) Dhinojwala, A.; Torkelson, J. *Macromolecules* **1994**, *27*, 4817.

(27) Liu, Y. S.; Ware, W. R. *J. Phys. Chem.* **1993**, *97*, 5980.

(28) Soutar, I.; Phillips, D.; Roberts, A. J.; Rumbles, G. *J. Polym. Sci., Polym. Phys. Ed.* **1982**, *20*, 1759.

(29) Kamat, P. V. *Anal. Chem.* **1987**, *59*, 1636.

(30) Yuan, H. L.; Párkányi, C.; Guo, R. K.; Wu, F. P. *J. Photochem. Photobiol. A: Chem.* **1992**, *63*, 45.

(31) Itagaki, H. *Macromolecules* **1991**, *24*, 6531.

(32) Zhang, G.; Thomas, J. K. *J. Phys. Chem.* **1995**, *99*, 11203.

(33) Abuin, E. A.; Lissi, E. A.; Radic, D. *Eur. Polym. J.* **1980**, *16*, 793.

(34) Nishimoto, S.; Yamamoto, K.; Kagiya, T. *Macromolecules* **1982**, *15*, 1180.

(35) Hoyle, C. E., Torkelson, J. M., Eds. *Photophysics of Polymer Systems*; ACS Symposium Series; American Chemical Society: Washington, DC, 1987.

(36) Birks, J. B. *Photophysics of Aromatic Molecules*; Wiley-Interscience: New York, 1970.

(37) Jang, F. H.; Woo, E. M. *Polymer* **1999**, *40*, 2231.

(38) Woo E. M.; Su, C. C. *Polymer* **1996**, *37*, 4118.

(39) Berlman, I. B. *Energy Transfer Parameters of Aromatic Compounds*; Academic Press: New York, 1973.